# Subsurface structural mapping of Northern Nasser Lake region, Aswan, Egypt, using Bouguer data

## Salah SALEH[1]

[1] National Research Institute of Astronomy and Geophysics; Helwan, Cairo, Egypt;
 e-mail: salahsmm@yahoo.com

**Abstract:** In this study, we attempt to delineate the subsurface structures for the tectonic active region of Northern Nasser Lake using integrated interpretation techniques of gravity data with seismicity. The depths to the gravity sources, and the locations of the contacts of density contrast were estimated. Two methods were used for estimating source depths and contact locations: horizontal gradient (HG) and Euler deconvolution methods. Moreover, power spectral analysis, bandpass and upward continuation techniques were applied to evaluate the shallow and deep seated structures. Shallow depth structures were ranging between 0.30 km and 0.80 km. However, two average levels (interfaces) at depth 3.1 km and 7.2 km below the measuring level were revealed for the intermediate and deep seated structures respectively. Results of Euler deconvolution method suggested that, in the eastern part of the area, the basement could be observed on the ground and has become deeper in the central part. The interpreted structural map reveals that the area is affected by a set of faults trending mainly in the NW, E–W, N–S and NE–SW directions. Actually, this map has confirmed the idea that the intersections between the N–S and E–W striking faults along Nasser Lake area have generated seismic pulses. Moreover, three seismic zones (Z1, Z2 and Z3) are well correlated with the fault trends of the subsurface structures as derived from the horizontal gradient map. The present results suggest that there exist seismically-active fault east of High Dam, passing throughout Aswan reservoir from north to south. This fault is occupying region of high stress values which may generate large earthquakes in future, as it has long extension over several kilometers. Furthermore, the evaluated intruded volcanic bodies are found almost at the intersections between the E–W and NW oriented faults. Finally, the area is dissected by basement uplifts and troughs controlled mainly by the NW–SE faults.

**Key words:** Aswan reservoir Lake Egypt, Bouguer data, Euler deconvolution, horizontal gradient, power spectral analysis, filtering

## 1. Introduction

The study area is occupied by northern part of Nasser Lake (Fig. 1), which

has started to fill due to the Aswan High Dam construction early in 1964, and to form one of the largest man-made reservoirs in the world. It is extended over 500 km in southern Egypt and northern Sudan along the main course of the River Nile. The Aswan High Dam is considered as a unique structure among all large irrigation and electric power projects in the world. It was evident through previous geological and geophysical studies that Nasser Lake has affected the tectonic stability of the Aswan region, since water penetration through open fractures and other tectonically weak zones in the submerged land has significantly contributed to further fractur-
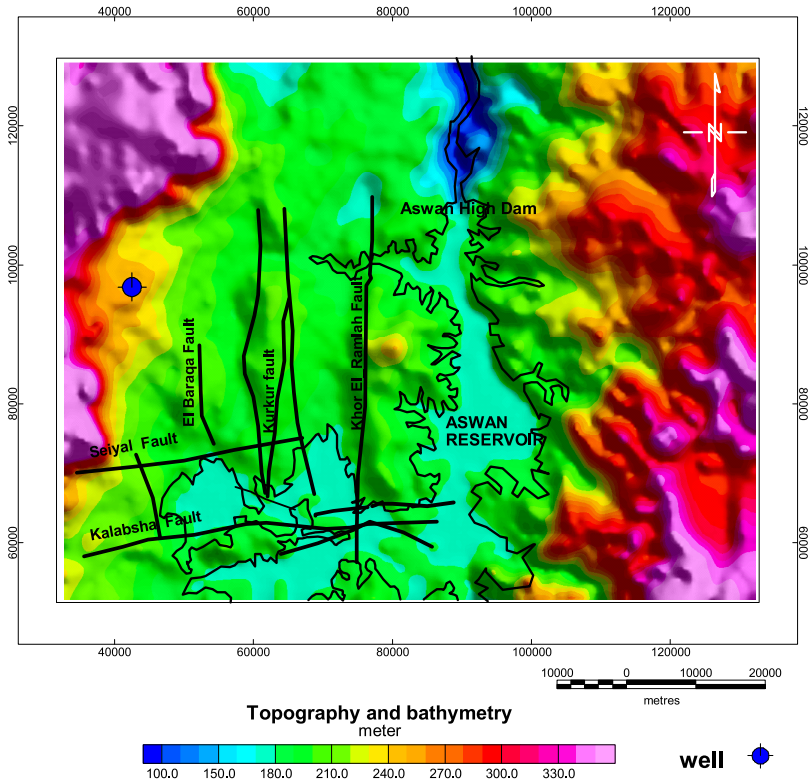


Fig. 1. Location map of the area of study. The E–W and the N–S fault systems are also shown. The location of subsurface lithologic log of drilled well (W1) is also shown (see Fig. 3).

ing and reactivation of some pre-existing faults (*Kamel and Elsirafe, 1993*).

The gravity method is one of the best geophysical techniques for delineating subsurface structures. The present study is based on qualitative and quantitative analysis of the gravity data to delineate both shallow and deep basement structures and present a new perspective on the subsurface structural setting at Nasser Lake area. For that purpose, the gravity data were subjected to spectral analysis in order to distinguish deep sources from shallow sources. The data were transformed to the frequency domain and regional/residual separation was made using bandpass filter based on the power spectrum. We attempt also to map the subsurface structure and estimate the depth to the basement and the location of some intruded (volcanic) bodies which erupted beneath the area of Nasser Lake (in the Upper Cretaceous era) during the regional uplift associated with the northern Red Sea rifting. This study is based on the analysis and interpretation of the Bouguer gravity data applications of gradients (filtering, horizontal gradient, and Euler deconvolution) and also on the available surface and subsurface geologic information. The advantage of these techniques is that they provide source location parameters using only a few assumptions.

As far as earthquakes are concerned, it is necessary to correlate between the seismicity and subsurface structures for seismic sources identification; especially if the study area includes the High Dam. As the population of Aswan is getting agglomerated in the form of urban clusters and great projects, the risk of economic and human loss due to seismic hazard is increasing. This study provides the seismic segments in north Aswan area, where the High Dam exists, as an important requirement for earthquake engineering and in seismic micro-zonation study.

## 2. Surface geology, structural setting and seismicity of the reservoir area

Nasser Lake overlies mainly the basement rocks (Precambrian rocks), which is outcropping on the eastern bank of the Lake. Igneous and metamorphic rocks made up the Precambrian formation (Fig. 2). The Nubian Sandstone is flat lying, relatively unreformed and gently dipping west, while it ranges in thickness from 250 to 400 m beneath the western extent of the reservoir
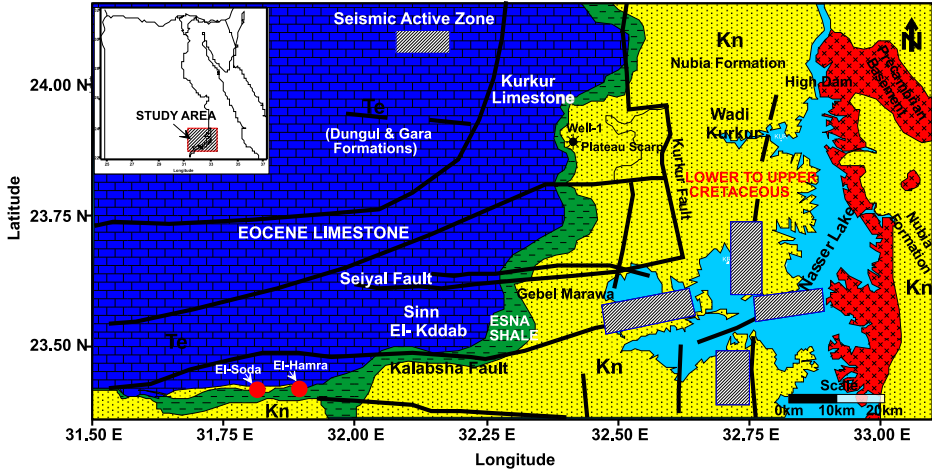
Fig. 2. Simplified geological map of the studied region (modified from *Issawi, 1969*). The active seismic zones are shown in the figures. Also, the location of subsurface lithologic log of drilled well (W1) is shown.

(*Issawi, 1969; 1978; 1982*). Most of the southwestern part of Aswan region is covered with forel and sediments ranging in age from Cretaceous to Quaternary, with some exposures of igneous and metamorphic rocks (Fig. 2). The sedimentary section in the studied area is thin and consists of a succession which unconformable overlies the basement rocks (Fig. 3). The studied area belongs to the stable shelf *(Said 1962)*. In other modified classification, it is included in the Archican Nubian shelf (*Meshref, 1990;* Fig. 4).

Structurally, the region is cut by a coupled set of E–W and N–S faults (Figs. 2 and 5), which appear to be vertical and extending into the granitic basement *(Issawi, 1978)*. These two sets intersect beneath the Gebel Marawa area (Fig. 2). The Kalabsha E–W fault strikes through the center of Wadi Kalabsha, passing south of the Limestone plateau (Sinn El-Kaddab plateau). The most prominent topographic feature in the Nubian plane is Gebel Marawa, an outlying remnant of the limestone plateau, which lies in a slight synclinal depression on the Kalabsha fault directly above the most active zone of seismicity (Fig. 5). A number of the synclines are found along the fault, associated with minor pull-apart structure, which may be related to the offset, strike-slip segments of the Kalabsha fault. Some of the fault trends show surface topographic expression as lineation of highly resistant

ridges. These ridges are formed of iron-rich material that permeates the fault zones. This material is of lower permeability than the surrounding sandstone, so that the fault segments may form vertical dykes and prevent horizontal water spreading towards west. The November 1981 earthquake and the subsequent seismicity have occurred mainly on the Kalabsha fault trends, beneath the largest embayment (Wadi Kalabsha), which extends westward 30 km from the main body of the reservoir.
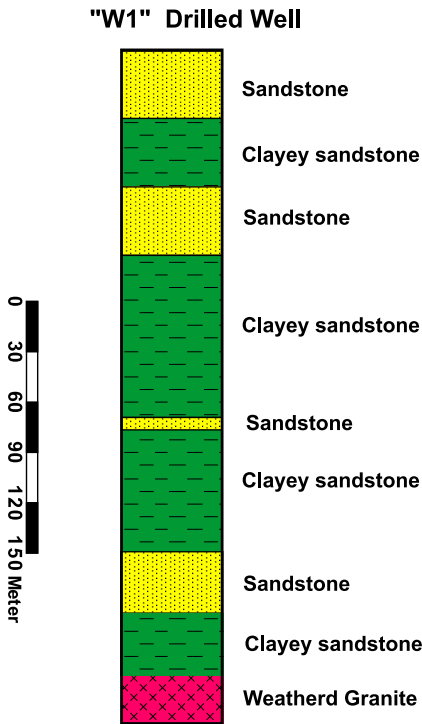


Fig. 3. Subsurface lithologic log of W1 drilled well (location is shown in Figs. 1 and 2).

The Aswan High Dam is located in a region of very infrequent earthquakes occurrence as revealed by the long historical record extending to Pharaonic times *(Kebeasy, 1990; WCC, 1985)*. On the other hand, instrumental catalogues report no events within 20 km around the Aswan area *(Kebeasy and Gharib, 1991)*. However, it appears that some low magnitude seismic activity may have occurred near the reservoir, after filling began and prior to November 1981 *(Kebeasy et al., 1982)*. On 14 November 1981, an earthquake of magnitude Ms = 5.3 took place in the Kalabsha area, followed by numerous aftershocks. Mainly, the seismicity of the area is concentrated along Kalabsha fault, including some seismic swarms occurred in 1982, 1983, 1984 and 1987.

Seismic active zone of Aswan is the closest active seismic zone to the High Dam, the main project of Egypt that controls the electricity and irrigation. Because of the presence of the first local seismic network around the area, some detailed studies were carried out concerning the seismic activity in the area, for the safety purpose of the High Dam, e.g. *Mohamed (1997; 2001)*.

*Mohamed et al. (2008)* have modified the seismicity map of Aswan area
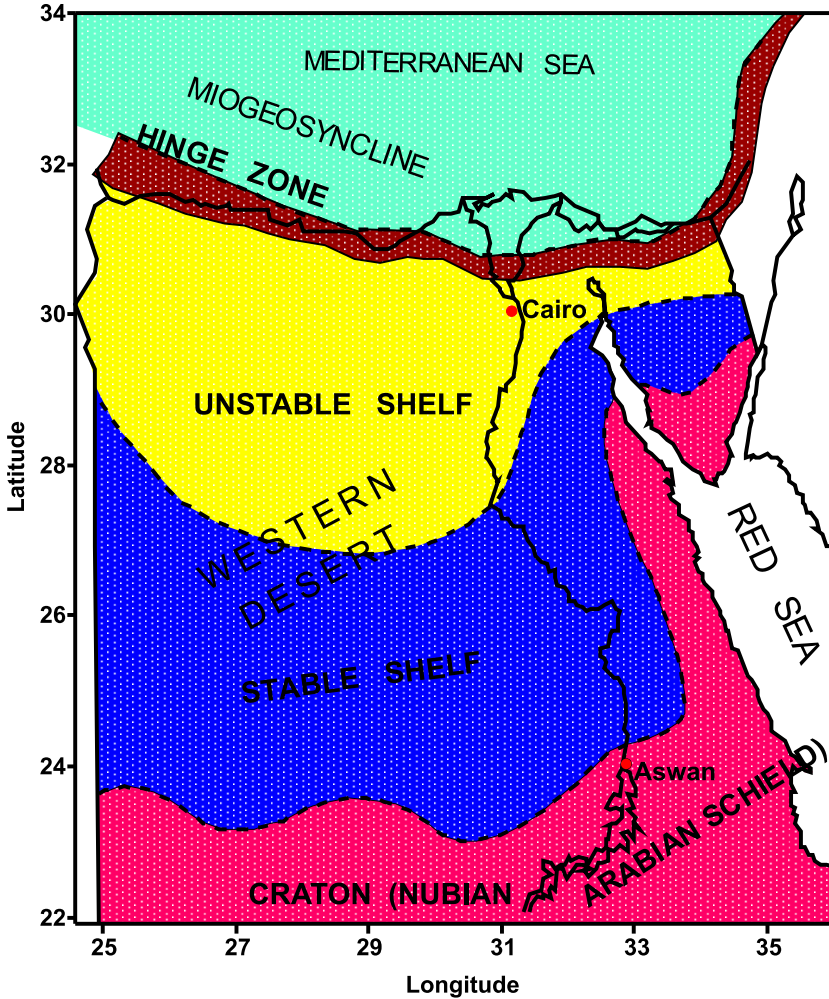
Fig. 4. Sketch of the structural aspects of Egypt (compiled after *Meshrif, 1990*).

during the period 1981–2006, which shows the following eight seismic clusters (Fig. 5); these zones were grouped according to spatial distribution and the level of the seismicity as what follows:

1 – West High Dam zone, 2 – Northern old stream channel zone, 3 – Southern old stream channel zone, 4 – Gable Marawa zone (GMR), 5 – East Gable Marawa, 6 – East – East Gable Marawa, 7 – Khor El-Ramla zone, 8 – Abu
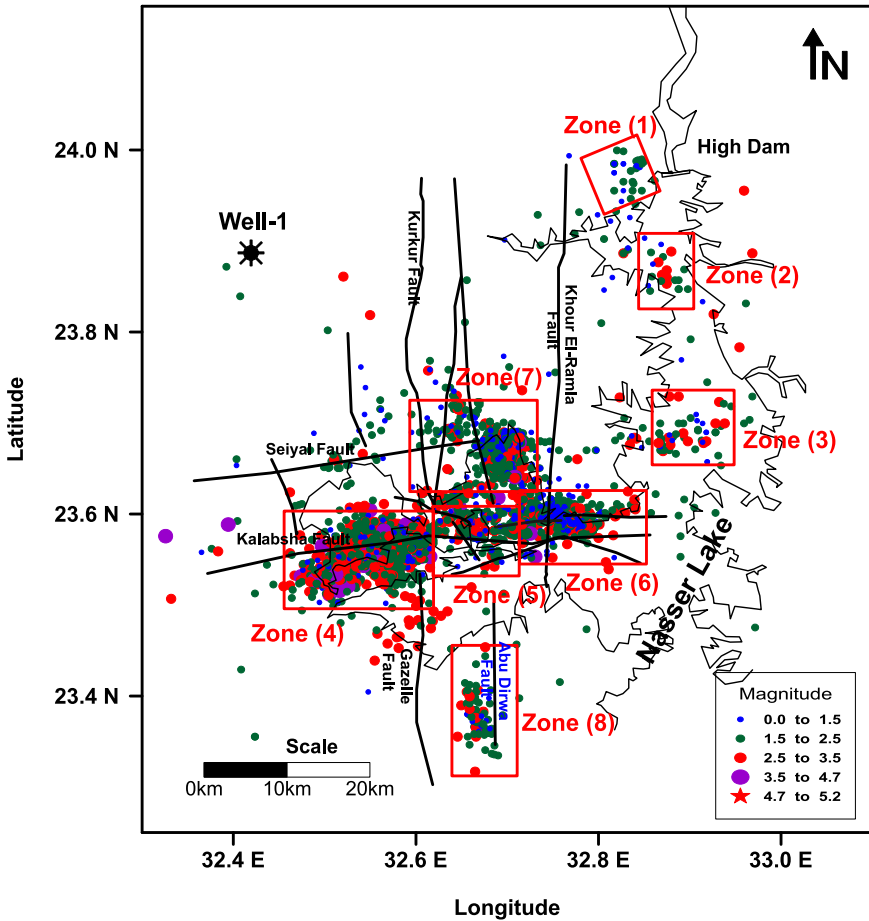
Fig. 5. Seismicity and the seismic zones in Aswan area from 1981 to 2009 (after *Mohamed et al., 2008*). The E–W and the N–S fault systems are shown in the figure.

Dirwa zone.

Some scattered micro-earthquakes are located in the Nile channel, zones (1, 2 and 3), they may associate a major north-south fault trend *(Youssef, 1968)*. However, Gable Marawa zone (GMZ, Zone 4) is the most active zone in Aswan region, which is located around the site of the Nov. 14, 1981 earthquake. Seismicity at this zone is characterized by a focal depth between 15–25 km.

Zone 5 lies to the east of GMR seismic zone and is characterized by a focal depth ranging from 2–7 km. To the east of zone 5, zone 6 is located; it is characterized by shallow seismic events, with the focal depth in the range of 1–3 km. The zone 7 is the second active zone in the area; it represents the activity along Khor El-Ramla fault beneath Khore El-Ramla depression, the edge of water container closet to the original channel (Fig. 5). It is characterized by a seismic activity of focal depth extending down to 8 km. Also, others are scattered around Abu Dirwa fault, representing zone 8.

## 3. Gravity data analysis

In 2000 National Research Institute of Astronomy and Geophysics carried out detailed gravity survey of the area surrounding the northern part of Nasser Lake using Lacoste-Romberg G-type gravitymeter with an accuracy of 0.01 mGal ($10^{-5}$ m/s$^2$). The elevation of gravity stations are measured using geodetic leveling and in some cases electronic altimeter with an overall accuracy of better than $\pm 0.2$ mGal in computed Bouguer anomaly. The gravity data is processed using IGSN, 1971, for a standard density of 2670 kg/m$^3$ for the Bouguer slab15. The overall accuracy of Bouguer anomaly map prepared from this data is about $\pm 0.01$ mGal and is good enough for the present study.

New Bouguer anomaly map was compiled for Aswan active region based on Bouguer data which have been surveyed in 1989 and 2000 by the National Research Institute of Astronomy and Geophysics (NRIAG, Fig. 6).

The compiled Bouguer gravity map (Fig. 6) is now available for evaluating subsurface structures using different techniques. This map can be divided into a number of distinct areas based on the anomaly size, trend and gradient, which can be related to the geological subsurface structures.

This map shows pronounced gravity highs and lows, representing the structural trends of this region. It remarkably shows the gravity gradients expressed by the faults of subsurface structures. The predominant trends of anomalies are generally striking in E–W, NW–SE and NE–SW directions.

The anomaly map depicts a northern gravity high (H1) with a relief of around –20 to –30 mGal coinciding with the northern part of High Dam with a width of nearly 15 km. Two other high anomalies (H2 and H3) with
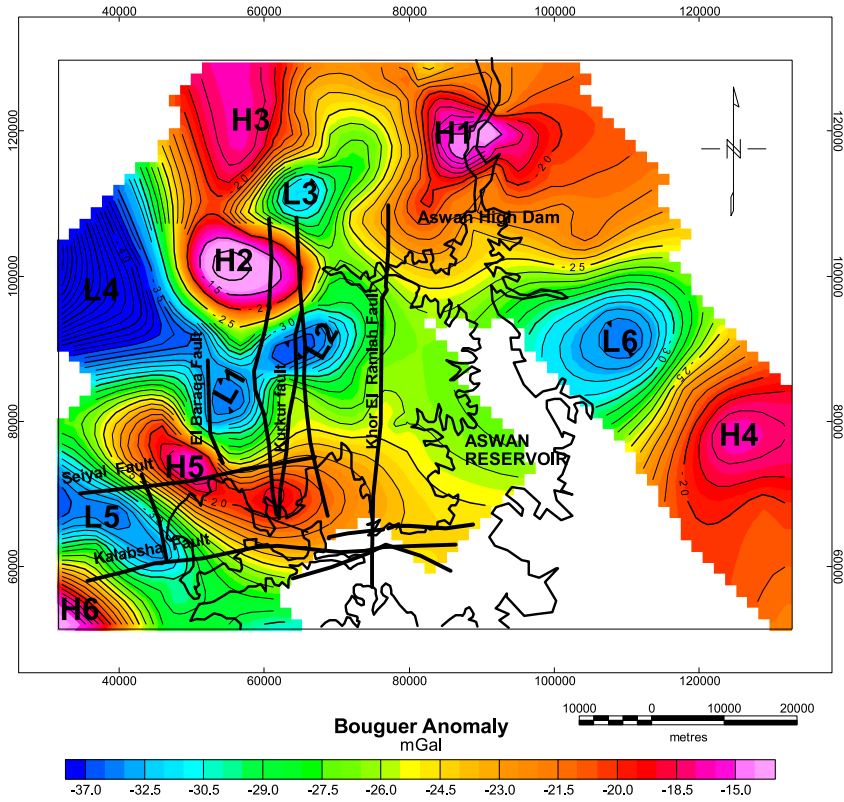
Fig. 6. Bouguer anomaly map of northern part of Nasser Lake. The E–W and the N–S fault systems are shown in the figure.

gravity values exceeding –15 mGal occupy the north western parts of the study region. Their trends are E–W and NNW–SSE, respectively.

A zone of negative gravity value extends in the western region containing three low anomalies, two of them (L1 and L2) form an elongated NE–SW negative gravity anomaly (–34 mGal).

Moreover, the third low anomaly (L3) is located at the northern end of Kurkur fault systems. Whereas the fourth low anomaly (L4) with a gravity value less than –35 mGals is trending in NW-SE direction as shown in Fig. 6. Further south an alternative gravity high and low anomalies were observed, covering Kalabsha and Seiyal active region in the southern western corner

for the region of study.

Eastern area of Nasser Lake is occupied by negative low anomaly (L5) striking in NE–SW direction. This low gravity zone has a Bouguer anomaly value of about –30 mGal. The circular gravity highs (H1) and (H2) with a relief of around mGal is pointing out the existence of intrusive bodies in this area, similar to volcanic plugs of Aswan active region and coincidentally these highs are located near the epicenters of the most earthquakes in this region.

## 3.1. Spectral analysis and filtering of gravity data

The power spectral analysis yields the depths of significant density contrasts in the crust, where there is little information on the crustal structure. *Spector and Bhattacharyya (1966)* studied the energy spectrum calculated from different 3-D model configurations; Spector and Grant (1970) studied the statistical ensemble of 3-D maps. They concluded that the general form of the spectrum displays contributions from different factors and can be expressed as:

$$E(r, \vartheta) = \langle H(h, r) \rangle \langle S(a, b, r, \vartheta) \rangle \langle C(t, \Phi, r) \rangle, \tag{1}$$

where
$E$ – total energy;
$r = 2\pi(f_x^2 + f_y^2)^{1/2}$ – radial wave number ($r = 2\pi f$, where frequency $f$ can be measured in any direction in the $x$-$y$ plane);
$\theta = tan^{-1}(f_x/f_y)$ – azimuth of the radial wave number;
$\langle \rangle$ – expresses ensemble average;
$h$ – depth;
$H$ – depth factor;
$S$ – horizontal size (width) factor;
$C$ – vertical size (thickness or depth extent) factor;
$a, b$ – parameters related to the horizontal dimensions of the source;
$t, \Phi$ – parameters related to the vertical depth extent of the source.

It is clear that only three factors ($H, S,$ and $C$) are functions of the radial frequency $r$; thus in the case of profile form, Eq. (1) can be written as:

$$\ln E(q) = \ln H(\bar{h}, q) + \ln S(\bar{a}, q) + \ln C(\bar{t}, \Phi, q) + \text{constant}, \tag{2}$$

where $\bar{h}, \bar{a}, \bar{t}$ are the average depth, half width and thickness of a source ensemble, and $q = 2\pi f$.

This equation demonstrates that contributions from the depth, width and thickness of a source ensemble can affect the shape of the energy spectral decay curve. The effect of each factor has been discussed in the literature. The result of the spectral analyses of Bouguer anomaly of Aswan active region is shown in Fig. 7a. The distinguishing feature of the logarithmic decay energy curve shows the rapid decrease of the curve at low wavenumbers, which is indicative of response to deeper sources. The gen-
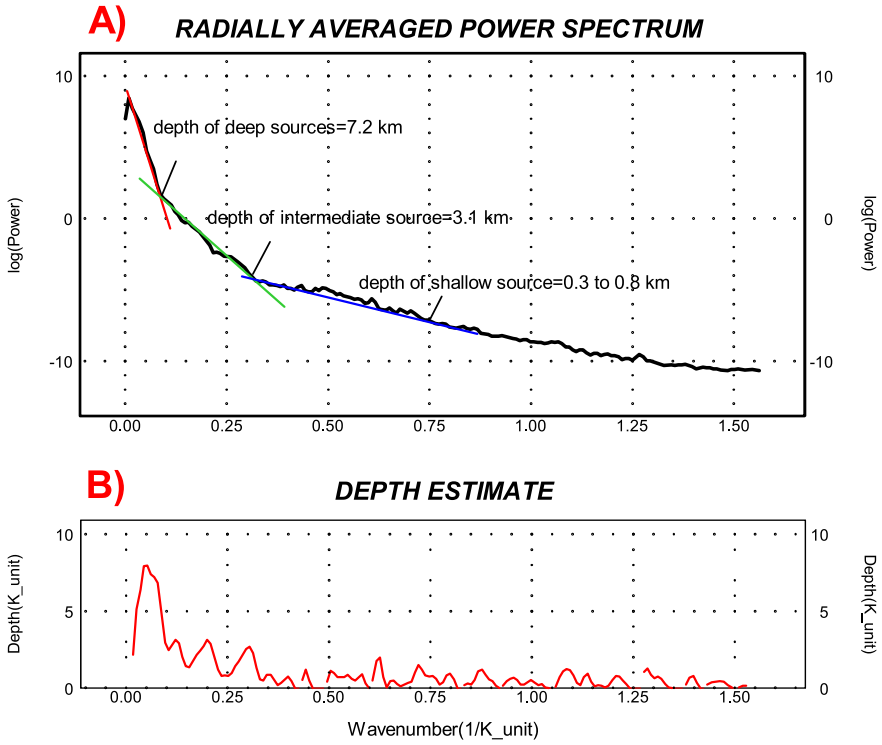


Fig. 7. A) An example of a radially averaged power spectrum of the Bouguer anomalies of Aswan region. The spectrum shows straight line segments, which correspond to 'ensembles' of density bodies with the same average depths of layers using the gradient of the straight segments unless the average width of the anomalies in the ensembles is known. B) Gravity depth estimation based on averages of the slope of the energy spectrum.

tler decline of the remainder of the curve relates to the near-surface sources. The spectrum consists essentially of three components: a very steep part at low wavenumbers ($0$ km$^{-1}$ $\leq$ wavenumber $\leq 0.0750$ km$^{-1}$) and a less steep part at moderate wavenumbers ($0.075$ km$^{-1}$ $\leq$ wavenumber $\leq 0.325$ km$^{-1}$). Moreover, a gentle part at high wavenumbers ($0.325$ km$^{-1}$ $\leq$ wavenumber $\leq 1.55$ km$^{-1}$) was observed. This negative asymptotic character shows that the gravity data has three components:

- A regional component of long wavelength from deep-seated sources.
- An intermediate component of middle wavelength from intermediate-seated sources.
- A local component caused by sources at shallow depth, e.g., basement and/or volcanic rocks.

Between $0$ km$^{-1}$ and $0.0750$ km$^{-1}$, the contribution of the regional component decreases as the wavenumber value increases at the near-surface component. At wavenumber equal to $1.050$ km$^{-1}$, the curve describes the noise, produced by the digitization errors and finite sample interval, as fluctuations about a constant level of energy. The depth of the gravity sources can be estimated and the field components can be separated by bandpass filtering of the field.

## 3.2. Effect of the source depth

The depth to the source ensemble is the main factor which controls the shape of the energy spectral decay curve. It is expressed as

$$H(\bar{h}, q) = e^{2\bar{h}q}. \tag{3}$$

Depths to deeper and shallower sources are described by the decay slopes of the curve at lower and higher frequencies, respectively. The slope of the line fitted to any linear segment of the curve can be used to compute either the depth to the causative source or the mean depth to a corresponding group of sources having comparable depths.

It is clear from Eq. (2) that if $S = C = 1(a > \bar{h}$ and $t < \bar{h})$, then the equation will be reduced to

$$\ln E(q) = \ln H(\bar{h}, q) + \text{constant}, \tag{4}$$

but from Eq. (3)

$$\ln H(\bar{h}, q) = -2\bar{h}q. \tag{5}$$

Hence the depth to the top of the source ($\bar{h}$) can be computed from the slope as follows: $\bar{h} = -s/2$ if $E$ is plotted against $q$ or $\bar{h} = -s/4\pi$ if $E$ is plotted against $f$.

$\bar{h}$ is the depth, $s$ is the slope of the log (energy) spectrum and $q$ is the wavenumber at frequency $f$ (spatial frequency), where $slope = \ln E(q)$ and $q = 2\pi f$.

Two different approaches can be used to interpret the investigated depth: 1) the point average calculation from the slope of the energy curve; 2) the linear segments of the energy decay curve, with distinguishable slopes, that are attributed to contributions in the gravity data from sources at various depths, which is used in this paper. Figure 7b shows the gravity depth estimated from the power spectral analyses of Bouguer anomaly of Aswan region. Three different layers can be separated: the first layer is characterized by the near surface contribution, the depth may vary from 0.3 to 0.8 km; the second layer is characterized by the intermediate-seated contributions, the depth is from 0.8–3.1 km and the deep-seated contribution, the depth may change from 3.1. to about 7.2 km depth. The estimated depth value of deep seated structures (the high velocity layer) using this technique is well correlated with 3D velocity structural results of *Haggag et al. (2009)*.

## 3.3. Horizontal gradient (HG) gravity map

The horizontal gradient method has been used intensively to locate boundaries of density contrast from gravity data or pseudogravity data stated that the horizontal gradient of the gravity anomaly caused by a tabular body tends to overlie the edges of the body if the edges are vertical and well separated from each other *(Cordell, 1979; 1985)*.

The gravity data were employed for making interpretations about subsurface geology in terms of density contrast, which is typically not directly recognized on the surface. Analysis of the gravity data contributes to imaging the subsurface structure of the study area. As such, two filters were

used in order to enhance the gravity, including the horizontal gradient filter and the Euler deconvolution. The horizontal-gradient method has been used since 1982 to locate density/magnetic boundaries from gravity data or pseudogravity data *(Cordell and Grauch, 1985)*. The method is based on the principle that a near-vertical fault-like boundary produces a gravity anomaly with a horizontal gradient that is largest directly over the top edge of the boundary.

The greatest advantage of the horizontal gradient method is that it is least susceptible to noise in the data, because it only requires the calculations of the two first-order horizontal derivatives of the field *(Phillips, 1998)*. The method is also appropriate in delineating both shallow and deep sources, in comparison with the vertical gradient method, which is useful only in identifying shallower structures. The amplitude of the horizontal gradient *(Cordell and Grauch, 1985)* is expressed as:

$$HG_g(x,y) = \sqrt{\left(\frac{\partial g}{\partial x}\right)^2 + \left(\frac{\partial g}{\partial y}\right)^2}, \tag{6}$$

where $\partial g/\partial x$ and $\partial g/\partial y$ and are the horizontal derivatives of the gravity field in the $x$ and $y$ directions. The amplitude of the horizontal gradient for the regional data of the Aswan area was calculated in the frequency domain and is illustrated in Fig. 8.

Generally, magnetic data can be transformed to pseudo-gravity data using Fourier techniques *(Blakely and Simpson, 1986)* such that they behave like gravity data. Thus, the horizontal gradient of pseudo-gravity also has a maximum magnitude directly over the boundary. The horizontal gradient contour lines mark the top edges of magnetic or density boundaries.

In this study, the horizontal gradient filter provides high values over the faults or contacts. *Blakley and Simpson (1986)* proposed a method to select the highest values of the gridded data at which the faults or contacts are located.

Figure 8 shows the horizontal gradient map for the gravity data in the study area using Fourier techniques *(Blakely and Simpson, 1986)*. The blue lines represent the boundaries/contacts that were interpreted from the map. The interpreted structural map using HG reveals that the area is affected by a set of faults trending mainly in the NW, E–W, N–S and NE–SW directions.

High gradient values were observed around the low gravity at north of Kalabsha active region extending to the northeastern side of the area of study. It is observed that the pattern of the high gradient anomalies is broad, not like the sharp anomalies of ideal vertical boundaries of contrast-
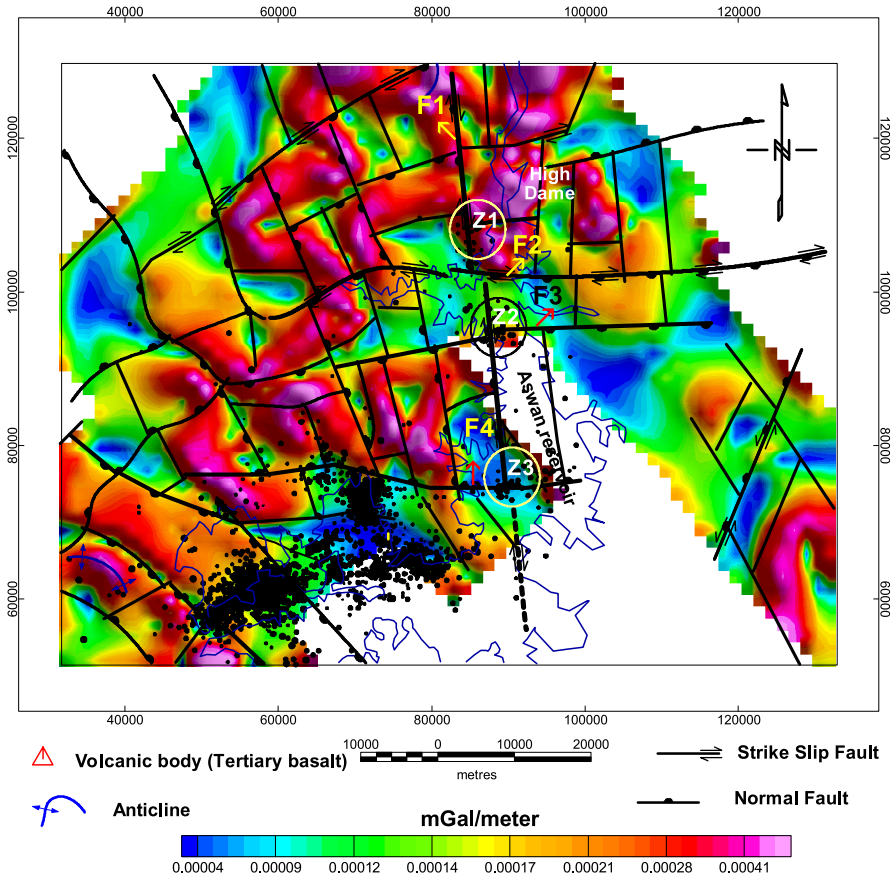
Fig. 8. The horizontal gradient map of the gravity data of Aswan active region. Black lines indicate the main active faults from previous studies, and the blue lines show the faults from the horizontal gradient filter based on the work of *Blakely and Simpson (1986)*. The inferred N–S trending fault (F1) intersects with three main significant E–W striking faults (F2, F3 and F4) which have generated seismic clustering (zones) around their intersections. Seismicity and the seismic zones Z1, Z2 and Z3, which are related to the same active fault trending in the N–S direction (F1) in the study region, are also shown.

ing density. One explanation of this pattern is that the boundaries in the north western part of Nasser Lake Aswan area are not vertical and are relatively deep, and/or the anomalies are produced by several boundaries.

*Grauch and Cordell (1987)* discussed the limitations of the horizontal gradient method for gravity data. They concluded that the horizontal gradient magnitude maxima can be offset from a position directly over the boundaries if the boundaries are not near-vertical and close to each other.

### 3.4. Euler deconvolution

The Euler deconvolution method is applied to the residual gravity data of Aswan active region from the range 0 to more than 3 km of depth. Euler deconvolution is used to estimate depth and location of the gravity source anomalies. The 3D equation of Euler deconvolution given by *Reid et al. (1990)* is

$$(x - x_0)\frac{\partial g}{\partial x} + (y - y_0)\frac{\partial g}{\partial y} + (z - z_0)\frac{\partial g}{\partial z} = -n(\beta - g). \tag{7}$$

Eq. (7) can be rewritten as

$$x_0\frac{\partial g}{\partial x} + y_0\frac{\partial g}{\partial y} + z_0\frac{\partial g}{\partial z} + n\beta = x\frac{\partial g}{\partial x} + y\frac{\partial g}{\partial y} + z\frac{\partial g}{\partial z} + ng, \tag{8}$$

where $(x_0, y_0, z_0)$ is the position of a source whose total gravity is detected at $(x, y, z)$, $\beta$ is the regional value of the gravity, and $n$ is the structural index (SI) which can be defined as the rate of attenuation of the anomaly with distance. The SI must be chosen according to prior knowledge of the source geometry. For example, SI = 2 for a sphere, SI = 1 for a horizontal cylinder, SI = 0 for a fault, and SI = –1 for a contact *(FitzGerald et al., 2004)*. The horizontal $(\partial g/\partial x, \partial g/\partial y)$ and vertical $(\partial g/\partial z)$ derivatives are used to compute anomalous source locations. By considering four or more neighboring observations at a time (an operating window), source location $(x_0, y_0, z_0)$ and ß can be computed by solving a linear system of equations generated from Eq. (8). Then by moving the operating window from one location to the next over the anomaly, multiple solutions for the same source are obtained. In our study, Euler deconvolution has been applied to the

gravity data using a moving window of 0.5 km × 0.5 km (grid space is 50 m).

We have assigned several structural indices values, and found that SI = 0 gives good clustering solutions. *Reid et al. (1990; 2003)*, and *Reid (2003)* presented a structural index equal to zero for the gravity field for detecting faults. Results of the Euler deconvolution for gravity data are shown in Fig. 9.

The High Dam region is the most folded area in Aswan region. This may be due to the existence of some shallow intruded bodies. Most of the contact solutions (Fig. 9) are trending in the NNW and NW directions,
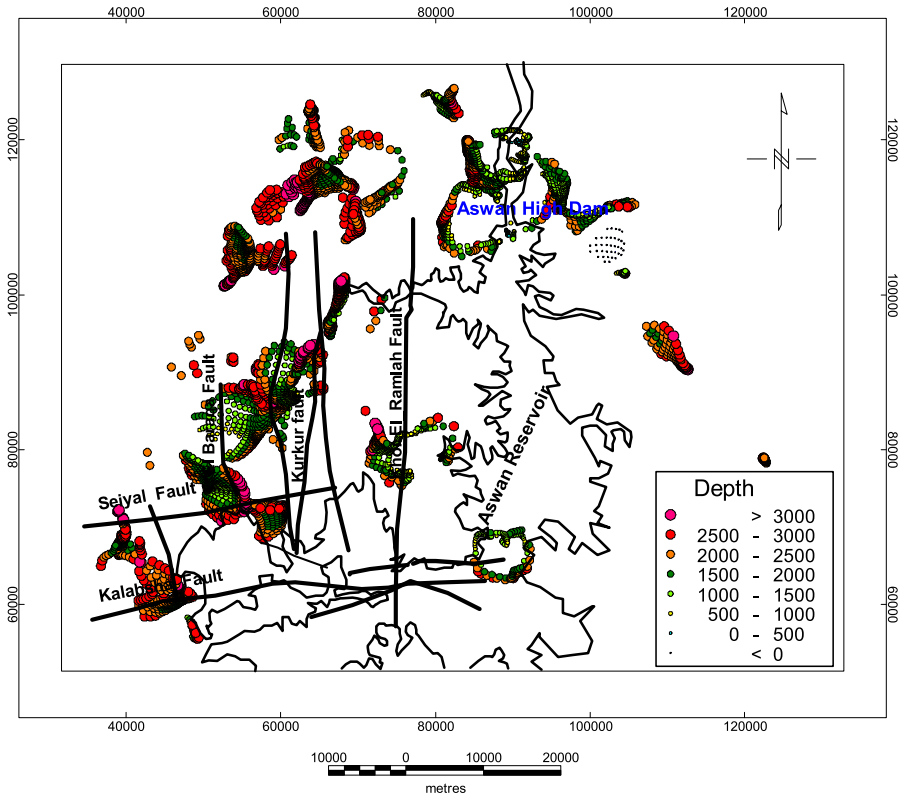


Fig. 9. Euler solutions from the residual gravity data of Aswan region. Structural Index = 0; tolerance = 15%; window size = 500 m× 500 m.

associated approximately with the main trend of the Red Sea. In a few locations, solutions are found to be trending in the NE–SW direction. This trend is related to the transformed faults, which is associated with the Red Sea rifting *(Said, 1992)*. Generally the solutions delineate boundaries of intrusive narrow density bodies scattered in the study area with different width and length. The wider one (6 km) with a length of 10 km is located around the High Dam. The depths associated with the Euler solutions for these bodies range between 1.2 km and about 3 km. These bodies are most probably representing intrusions that are associated with the Red Sea rift. Such scattered intrusions in the basement would be expected to produce structures higher up in the sedimentary section. We are currently investigating 3D modeling techniques to obtain more accurate information about the shape and density of the intruded bodies. Meanwhile, the depths estimated for the near-surface structures range from 250 to 1200 m, decreasing to the southeast of High Dam.

## 3.5. Upward continued gravity map

The resultant Bouguer anomaly map (upward continued at 7 km depth) is shown in Fig. 10. This map reflects many anomalies with different polarities and trends. In the western part of the study area (northwest of Seiyal and Baraka faults), it is represented by large amplitude of negative Bouguer anomalies (–31 to – 27.5 mGal), generally lineated in WNW–ESE direction. This may attribute to relatively thick sedimentary cover in this region. The central part of the study area is associated with relatively flat broad extended anomalies with extended values (–27 to –26 mGal) that strike in the E–W, direction. It is characterized by oval shape, low sharpness, and low gradient. This illustrates a continuous tectonic activity in this region (basin or the basement rocks seem to be of relatively acidic rock types intruded by basic ones probably of mantle composition at different depth). Moreover, three broad elongated positive anomalies of different closures that strike in the N-S, NNE–SSW and NE directions are observed in different sites of the Regional Bouguer map that occupying northern part of Kurkur fault, around Aswan High Dam to the north and in the south eastern corner of the studied region, respectively.
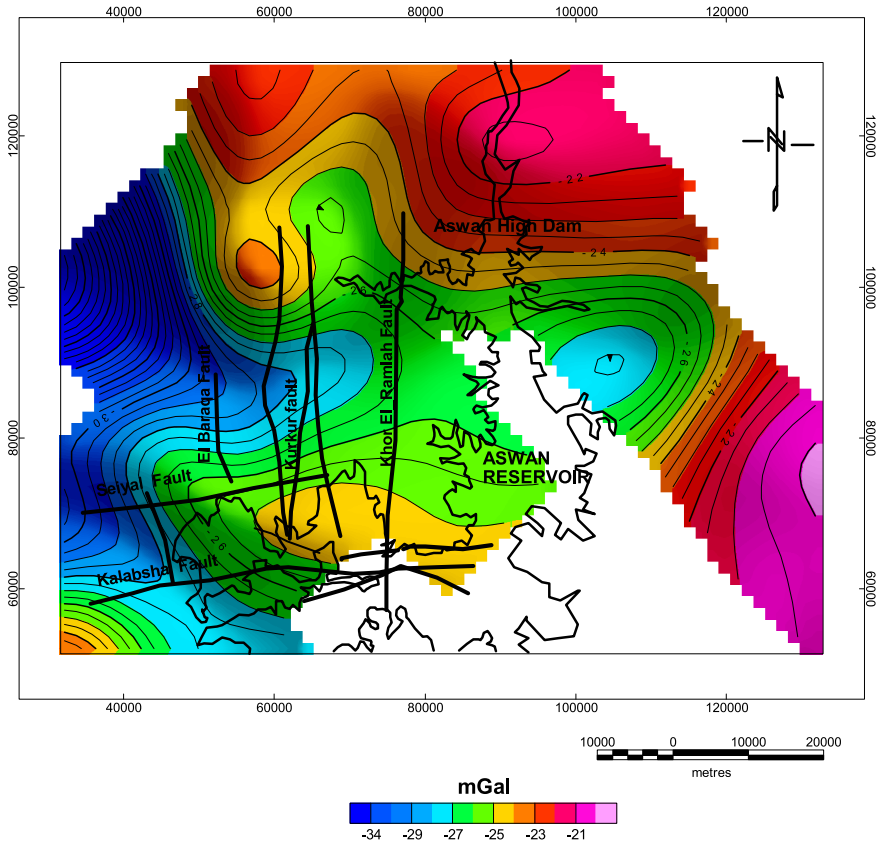
Fig. 10. Regional anomaly map of the study area deduced from upward continuation to a level of 7 km.

## 3.6. Bandpass filtered gravity map

An important step in the interpretation of Bouguer data is the study of the anomaly of a special shape. Linear anomalies correspond to dikes and (or) faults, and circular anomalies correspond to intrusive bodies. The structural elements can be detected simply by inspecting the alignment of anomalies and by distinguishing the noticeable abrupt change between positive and negative anomalies, particularly at the location of sharp gradients. The enhancement of Bouguer anomalies associated with faults and other structural

discontinuities (volcanic or intruded bodies) was achieved by the application of bandpass filter of the Bouguer data.

Most of the volcanic rocks are exposed on both flanks of the Nile Valley rift whereas the rift trough has less and scattered volcanic bodies. The Nile Valley rift and the other continental rifts, such as Taupo rift of North Island, New Zealand; Rungwe volcanic field and parts of the western arm of the East African rift system are characterized by the flank volcanism.

*Ellis and King (1991)* attribute the occurrence of the flank volcanisms to the dilation strain at the base of the upper crust during normal faulting and to uplift of the rift flanks at depth.

Continental rifts do not usually form single, straight structural entities, but they occur commonly as systems of isolated rift segments, which are separated by several transfer zones (*Corti et al., 2003* and *Corti, 2004*). In the Nile Valley rift, the interactions between the pre-existing faults have controlled the volcanic activity at and around the transfer zones (Fig. 11).

Bandpass filter parameters have been selected (0–5 km) after extensive testing of several bandpass ranges which was well fitted with the estimated source depth values using other techniques in this work. Figure 12 shows the bandpass filtered map, of Bouguer map overlain with interpreted structural aspects and intrusions. The map shows some intruded bodies which were observed scattered on the intersections between the E–W and NW oriented faults. These bodies tend to be aligned along NE trending direction as shown in Fig. 12 [related to the transformed faults, which is associated with the Red Sea rifting *(Said, 1992)*].

## 4. Interpreted structure map

The results (locations and depths) obtained from the data analysis were compared and integrated to construct the basement tectonic map (Fig. 13). The deep-seated structures, interpreted from the regional map, are displayed in bold black lines. Most of these structures are traced in confirmation by all Bouguer analysis methods. However, some structures were interpreted following the disruption and discontinuity of the method's solutions.

The near-surface lineaments and anticline folds are shown in blue lines, were traced by the application of the analysis methods to the residual component map. These lineaments show good agreement with the geologically
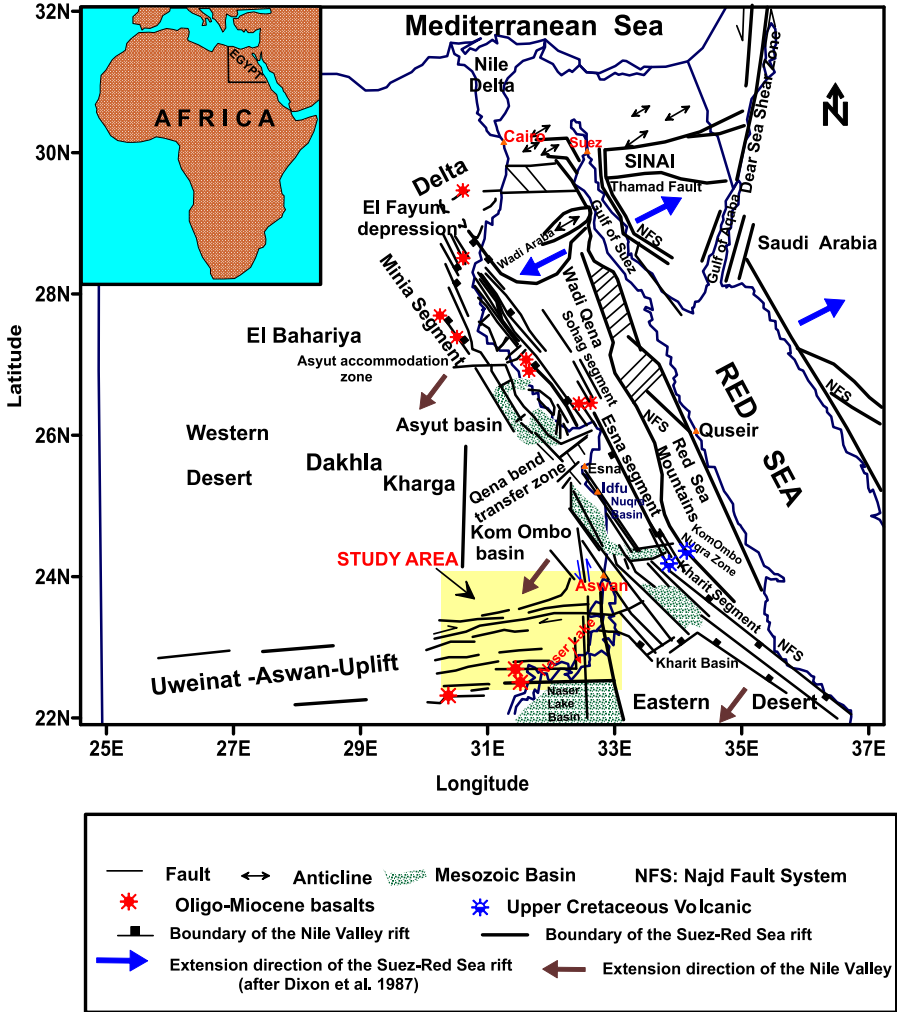
Fig. 11. Structures map of the eastern part of Egypt showing the Nile Valley rift and its internal Mesozoic basalt (modified after *Abd-Allah, 2008*). The Location of the Nasser Lake basins after *Taha (1992)* is represented. Red stars are the locations of Basaltic intrusions.

mapped linear features and main valleys cut across the area (Fig. 2). Accordingly, these lineaments might reveal top basement and intra-sediment
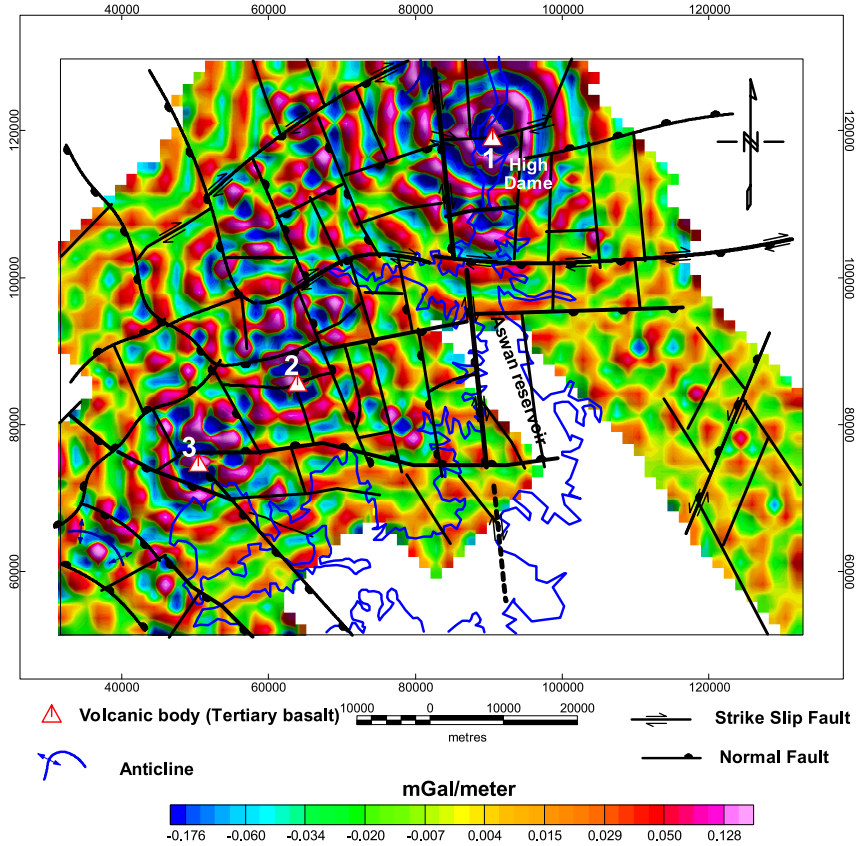
Fig. 12.   1–7 km band-pass filter of Bouguer anomaly map overlain with interpreted intrusions. The white triangles and circles mark location of volcanoes identified from filtered map. Strike slip and normal dextral oblique faults were estimated using all gravity techniques in this study.

structures.

Close inspection of the interpreted structure map (Fig. 13) reveals that the area is affected by four sets of deep-seated and near-surface structural lineaments oriented in NW–SE, E–W, N–S and NE–SW directions. The NW–SE (Red Sea) trend is more strongly developed than the other identified trends. It represents the prevailing tectonic trend in the area, and played an important role in the formation of its tectonic framework. It was
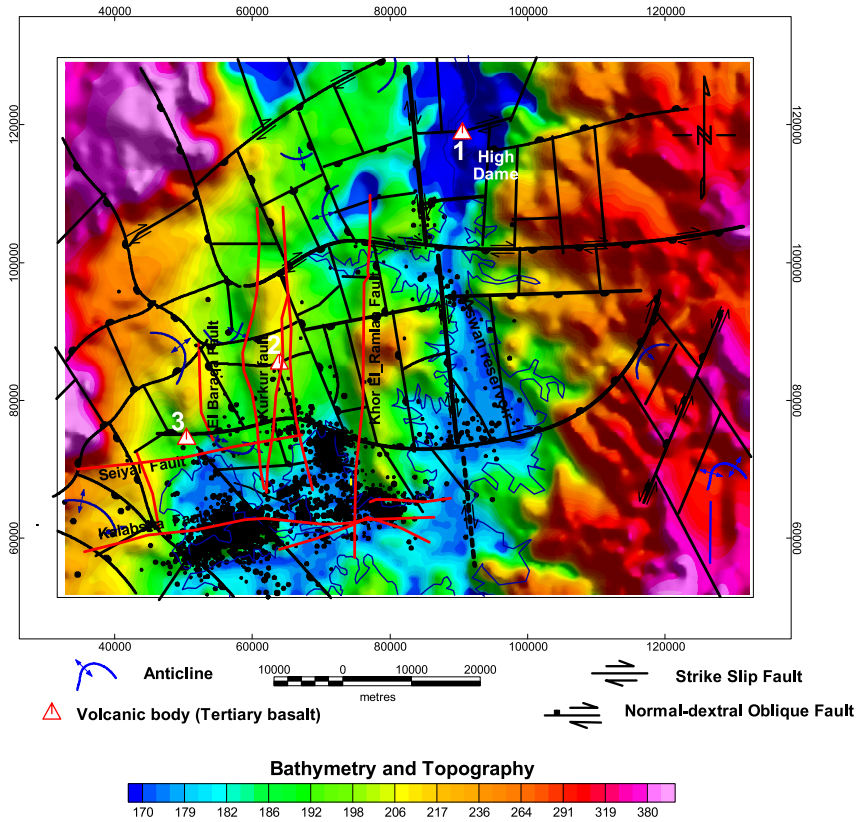
Fig. 13. Interpreted deep-seated (solid black lines) structural map. Blue lines are anticlines; while the red lines are the previous investigated faults (after *Issawi, 1969*). The estimated map shows E–W oriented faults and their relationship with the N–S and NW trending faults. White triangles (1, 2 and 3) mark location of volcanoes identified from filtered map. Earthquake distributions with black colored circles are also observed.

noticed that this trend is greatly responsible for the formation of the major basin that trends in the same direction and occupies the western and southwestern parts of the area. *Kamel and Elsirafe (1993)* stated that the NW and N–S trends represent the prevalent directional orientations of the surface structural lineaments in north Nasser lake area.

The E–W (Tethyan) and N–S (East African rift System) trends come in the second precedence as deep-seated and near-surface structures in the

67

study area. These two trends have been proved from interpretation of gravity survey data to be the deepest and oldest Precambrian tectonic trends in south Egypt. The E–W trend is represented by boundaries of uplifted and subsided blocks. The N–S trend is represented by strike slip faults affecting the central and eastern parts of the area and dislocating the E–W trending structures. This fault system is well identified in the area and extended for long distance northward controlling the primary extent of Nasser Lake and Nile valley in Upper Egypt. These tectonic trends have been shown to have a significant control on the distribution of seismic activity in the Aswan region. Most of the recorded earthquake activities in the western side of Nasser Lake are associated with the intersections of these two trends *(El Shazly and Abdel Hady, 1984; Kebeasy et al., 1987; Kamel and Elsirafe, 1993)*.

The NE trend is common in the interpreted near-surface structure in good agreement with the geologic map (Fig. 2). However, this trend is relatively scarce in the interpreted deep-seated structure. The E-W oriented faults are associated with several Oligocene and Miocene volcanic cones and dikes *(Schandelmeier et al., 1987; Meneisy, 1990)*.

The obtained results imply the estimation of some volcanic bodies (triangles 1, 2 and 3, Fig. 12) which have almost found at the intersections between the E–W and NW oriented faults.

The intersections between the N–S and E–W striking faults in the area around Nasser Lake have generated seismic pulses *(Kebeasy, 1990)*. Actually, the acquired results are almost identical with the previous statement, where the inferred N–S trending fault (F1) intersects with three main significant E–W striking faults (F2, F3 and F4) generating seismic clustering around their intersections as shown in Figs. 8 and 12.

## 5. Discussion and conclusions

In this paper, quantitative and qualitative analysis techniques were applied to Bouguer and seismicity data to estimate the location and depth of the buried source and subsurface structural interpretation. These techniques are power spectrum, horizontal gradient, Euler Deconvolution, upward continuations and bandpass filtering.

These methods were then applied to obtain the regional and residual components of the gravity field for the area of study. The HG method could map the deep-seated and near-surface density structure of the study area. The Euler solutions provide tracing of linear segments and the depth to these features. Results of Euler Deconvolution method suggested that on the eastern part of the area, the basement could be observed on the ground (50 m over the ground) and has become more deeper in the central part to attain more than 3 km depth to the west. This illustrates a continuous tectonic activity in this region (basin with thick sedimentary cover or the basement rocks seem to be of relatively acidic rock types intruded by basic ones probably of mantle composition at different depth).

Shallow depth estimation to the top of basement complex and/or intrusions is ranging between 0.3 km and 0.8 km. However, two average levels (interfaces) at depth 3.1 km and 7.2 km below the measuring level were revealed for the intermediate and deep seated structures, respectively.

Mostly, epicenters are located on the borders between the high and low Bouguer anomaly values. Seismic activity is concentrated along eight defined seismic active zones (Z1-Z8, see Fig. 5), where Zone4 is the most active one in Aswan region, where it is located around the site of the Nov. 14, 1981 earthquake. Seismicity distributions depicted that some low magnitude seismic activity may have occurred near the reservoir, after filling began and prior to November 1981 *(Kebeasy et al., 1982)* which led to occurrence of seismic pulses around seismic zone1 (Fig. 8). An additional two scattered micro-earthquakes (were distributed in zone 2 and zone 3, extending to the south) are located in the Nile channel.

In the present work, the three seismic zones (Z1, Z2 and Z3 as shown in Figs. 5 and 8) are well correlated with the fault trends of the subsurface structures as derived from the Horizontal Gradient map (Fig. 8) and also from Fig. 13 (tectonic of the basement rocks). These active zones are related to the same active fault trending in the N–S direction (F1). The inferred major fault trend-F1 depicted in Fig. 8, is well correlated with the major north-south structural trend discussed by *Youssef (1968)*.

*Saleh (2004)* estimated the resultant stress values for the same area of study using seismological and Bouguer data analyses. The estimated high stress anomalies values were occupying the northern, northwestern and eastern regions, which may not be related to any co-seismic and/or post seismic

movements. However, the seismic active zones have been located in the brittle zone over the low stress ductile one (along Kalabsha active region). Application of two geophysical methods in this paper such as seismicity and Bouguer analysis are strongly suggesting that seismically-active fault exists east of High Dam passes across Aswan reservoir from north to south. This fault is occupying a region of high stress value *(Saleh, 2004)* which may generate large earthquakes in future as it has long extension over several kilometers.

Integration of the results attained from these methods facilitates mapping the interpreted basement tectonic map of the area. This map shows that the area is affected by sets of faults trending in NW–SE, E–W, N–S and NE–SW directions. Moreover, the area is dissected by a set of basement uplifts and troughs controlled mainly by the NW–SE faults.

# References

Abd-Allah A. M. A., 2008: Structural evolution of the intercontinental Nile Valley rift, Egypt. J. Appl. Geophys., **7**, 1, 49–75.

Blakely R. J., Simpson R. W., 1986: Approximating edges of source bodies from magnetic or gravity anomalies. Geophysics, **51**, 7, 1494–1498.

Cordell L., 1979: Gravimetric expression of graben faulting in Santa Fe Country and the Espanola Basin, New Mexico, New Mexico. Geol. Soc. Guidebook, 30th Field Conf., 59–64.

Cordell L., Grauch V. J. S., 1985: Mapping basement magnetization zones from aeromagnetic data in the San Juan Basin, New Mexico. In Hinze W. J., Ed.: The utility of regional gravity and magnetic anomaly maps. Soc. Explor. Geophys., 181–197.

Corti G., 2004: Centrifuge modeling of the influence of crustal fabrics on the development of transfer zones: insights into the mechanics of continental rifting architecture. Tectonophysics, 384, 191–208.

Corti G., Bonini M., Conticelti S., Innocenti F., Manetti P., Sokoutis D., 2003: Analogue modeling of continental extension: a review focused on the relations between the patterns of deformations and the presence of magma. Earth-Science Reviews, 63, 169–247.

Dixon T. H., Stern R. J., Hussein I. M., 1987: Control of Red-Sea rift geometry by Precambrian structures. Tectonics, 6, 551–571.

El Shazly E. M., Abdel Hady M. A., 1984: Earthquake studies in Aswan environs, Egypt, applying space-borne imagery interpretation and other techniques. Remote Sensing Center, Academy of Scientific Research and Technology, Cairo, Egypt.

Ellis M., King G., 1991: Structural control of flank volcanism in continental rifts. Science, 254, 839–842.

Grauch V. J. S., Cordell L., 1987: Short note, Limitations of determining density or magnetic boundaries from the horizontal gradient of gravity or pseudogravity data. Geophysics, 52, 118–121.

Haggag H. M., Pankaj M., Bhattacharya S., Kamal, Kayal J. R., 2009: Seismicity and 3D velocity structure in the Aswan Reservoir Lake area, Egypt. Tectonophysics, 476, 450–459.

Issawi B., 1969: The Geology of Kurkur-Dungul area. General Egyptian Organization for geological Research and Mining. Geological Survey, Cairo, 46 p.

Issawi B., 1978: Geology of Nubia west area, Western Desert. Annuls of the Geological Survey of Egypt.

Issawi B., 1982: Geology of the southwestern desert of Egypt. Ann. Geol. Survey Egypt.

Kamel A. F., Elsirafe A. M., 1993: Delineation and analysis of the surface and subsurface structural lineament patterns in the North Lake Nasser area and its surroundings, Aswan, Upper Egypt. Int. J. Remote Sensing, **15**, 7, 1471–1493.

Kebeasy R. M., 1990: Seismicity. In: Said R. (ed.), Geology of Egypt. Rotterdam, 51–59.

Kebeasy R. M., Gharib A. A., 1991: Active faults and water loading are important factors in triggering earthquake activity around Aswan Lake. J. Geodynamics, 14, 73–85.

Kebeasy R. M., Maamoun M., Ibrahim E., 1982: Aswan Lake induced earthquakes. Bull. Int. Inst. Seismology and Earthquake Engng., Japan, 19, 155–160.

Kebeasy R. M., Maamoun M., Ibrahim E., Megahed A., Simpson D. W., Leith W. S., 1987: Earthquake studies at Aswan reservoir. In: Recent crustal movement in Africa. Edited by A. M. Wassef, Boud A., Vyskocial P. V.: Journal of Geophysics, 7, 173–193.

Meneisy M., 1990: Volcancity. In: Said R. (Ed.), The geology of Egypt, Balkema Rotterdam, 157–174.

Meshref W. M., 1990: Tectonic framework. In: Said R. (Ed.), The Geology of Egypt, A. A. Balkema, Rotterdam, 113–155.

Mohamed H. H., Gaber H. H., Sayed A. D., EZZAT M. E., 2008: A review of the recent seismic activity in the southern part of Egypt (Upper Egypt). Acta Geodyn. Geomater., **5**, 1 (149), 19–29.

Mohamed H. H., 1997: A study about the characteristics of the seismic activity at Kalabsha area and Aswan reservoir, Aswan. Ph. D. thesis, Qena Faculty of Science, South Valley University.

Mohamed H. H., 2001: Focal mechanism determination based on the polarity and sv/p amplitude ratio in the Kalabsha area, Aswan Egypt. Geosciences Journal, **5**, 2, 165–171.

Phillips J. D., 1998: Processing and interpretation of aeromagnetic data for the Santa Cruz Basin-Patahonia Mountains area, South-Central Arizona, U. S. Geological Survey Open-File Report 02-98.

Reid A. B., 2003: Short note, Euler magnetic structural index of a thin bed fault. Geophysics. Published electronically.

Reid A. B., Allsop J. M., Granser H., Millet A. J., Somerton I. W., 1990: Magnetic interpretation in three dimensions using Euler deconvolution. Geophysics, **55**, 80–91.

Reid A., FitzGerald D., McInerney P., 2003: Euler deconvolution of gravity data. SEG Annual Meeting, Dallas, accepted for presentation.

Said R., 1962: The Geology of Egypt. Elsevier Pub. Comp. Amsterdam and New York, 337 p.

Said R., 1992: The Geology of Egypt. Elsevier Science Ltd., Rotterdam, Netherlands.

Saleh S., 2004: Crustal stresses around the northern part of the Nasser Lake, Egypt as derived from gravity and seismological observations. NRIAG, Journal of Geophysics, Special Issue, 97–127.

Schandelmeir H., Richter A., Harms U., 1987: Proterozoic deformation of the east Sahran craton in SE-Libya, S-Egypt and N-Sudan. Tectonophysics, **140**, 233–246.

Spector A., Bhattacharyya B. K., 1966: Energy density spectrum and autocorrelation function of anomalies due to simple magnetic models. Geophysical Prospecting, **14**, 242–272.

Spector A., Grant F. E., 1970: Statistical models for interpreting aeromagnetic data. Geophysics, **35**, 293–302.

Taha A., 1992: Mesozoic rift basins in Egypt: their southern extension and impact on future exploration. Egyptian General Petrolum corpotion. 11th Exploration Conference, Egypt, 1–19.

WCC (Woodward-Clyde Consultants, 1985: Earthquake activity and Dam stability evaluations for the Aswan High Dam, Egypt, For the High and Aswan Dams Authority, Egypt, internal report, Subtask 1-G, 69 p.

Youssef M. I., 1968: Structural pattern of Egypt and its interpretation. Bull. Amer. Associ. Petroleum Geologists, **52**, 5, 60–614.